Clay Minerals, (2016) **51**, 445–455

Halloysite nanotubes with fluorinated cavity: an innovative consolidant for paper treatment

GIUSEPPE CAVALLARO, GIUSEPPE LAZZARA*, STEFANA MILIOTO AND FILIPPO PARISI

Department of Physics and Chemistry, Università degli Studi di Palermo, Viale delle Scienze, pad. 17, Palermo 90128, Italy

(*Received 15 October 2015; revised 12 December 2015; Guest Editor: Jock Churchman*)

ABSTRACT: Hybrid material based on halloysite nanotubes (HNTs) and sodium perfluorooctanoate (NaPF8) was used as a consolidant for paper treatment. The consolidation efficiency was determined by thermogravimetry as well as by paper grammage determination. Morphological analysis of the treated paper was performed by means of scanning electron microscopy while the effect of modified HNTs on the thermal behaviour of the cellulose fibres was investigated by differential scanning calorimetry which determined the combustion enthalpy of the paper. Water contact angle measurements were performed to study the paper wettability. The physico-chemical properties investigated (mesoscopic structure, thermal stability and wettability) of the treated paper were correlated successfully with the consolidation loading and, consequently, to the affinity between the fluorinated modified HNTs and the fibrous cellulose structure. This study proposes a new green protocol for paper consolidation based on natural tubular nanoparticles with a flame retardant effect.

KEYWORDS: thermogravimetry, differential scanning calorimetry, halloysite, wettability, paper.

In Cultural Heritage, the conservation of artworks based on paper represents a significant issue for both restorators and scientists. Deterioration of paper is affected by the degree of hydrolytic and oxidative reactions that occur upon aging. Moreover, the durability of cellulose fibres depends on the intrinsic composition/structure of the paper as well as on the conservation conditions, such as temperature and humidity (Havlínová *et al.*, 2009; Jana, 2009; Whitmore & Bogaard, 2009).

Recently, nanotechnology has been employed to improve the quality of paper documents by reducing their deterioration upon aging. Filling the fibrous structure of paper with nanoparticles such as magnetite, maghemite and ferrite generated materials with unique properties and functions (Shen *et al.*, 2010). The incorporation of silver nanoparticles in the cellulose structure induced the formation of new devices with antibacterial performances (Tankhiwale & Bajpai, 2009) which are essential to protect paper-based documents over time. The addition of montmorillonite and halloysite nanotubes (HNTs) into the cellulose structure improved the mechanical and thermal properties of the paper (Soares *et al.*, 2012; Cavallaro *et al.*, 2014a). Antibacterial paper with relevant tensile performance was obtained by incorporating montmorillonite into the cellulose structure (Soares *et al.*, 2012).

Among clay nanoparticles, HNTs are very promising because of their peculiar morphology and tunable surface chemistry (Joussein *et al.*, 2005). In addition, HNTs are biocompatible and non-toxic (Fakhrullina *et al.*, 2015). The particles of HNTs are polydisperse with lengths ranging between 0.1 and 2 μm, and with external and the inner diameters of ~50 and 15 nm, respectively (Lvov *et al.*, 2008; Pasbakhsh *et al.*,

* E-mail: giuseppe.lazzara@unipa.it
DOI: 10.1180/claymin.2016.051.3.01

2013). It was demonstrated that HNTs are appropriate nanomaterials for several appealing applications such as anticorrosive active coatings (Fix *et al.*, 2009; Joshi *et al.*, 2013), sustainable packaging (Cavallaro *et al.*, 2011a, 2013b; Gorrasi *et al.*, 2014) liquid crystals (Luo *et al.*, 2013), drug delivery (Vergaro *et al.*, 2012; Shutava *et al.*, 2014; Wei *et al.*, 2014) and decontamination (Zhao *et al.*, 2013; Cavallaro *et al.*, 2014c; Makaremi *et al.*, 2015). Filling polymeric matrices with HNTs enhanced the thermal stability and the tensile breaking strength of the pristine polymers (Cavallaro *et al.*, 2011a; Qiao *et al.*, 2012; Lvov & Abdullayev, 2013). Nanocomposites based on regenerated cellulose and HNTs showed excellent tensile properties because of the intertubular interactions between matrix and filler (Hanid *et al.*, 2014). Biocomposite films prepared *via* ionic liquids (Soheilmoghaddam *et al.*, 2013) and an aqueous casting method (Cavallaro *et al.*, 2011b) revealed well dispersed HNTs in a cellulose matrix. It was demonstrated (Liu *et al.*, 2013) that chitosan/HNT nanocomposites are proper scaffolds for tissue engineering. Within the Cultural Heritage field, a mixture of beeswax/HNTs was used successfully for the consolidation of waterlogged woods (Cavallaro *et al.*, 2015).

Here, an innovative green protocol for paper conservation was developed by using aqueous dispersions of modified HNTs as consolidants. In particular, HNT lumens were functionalized selectively by means of ionic exchange with sodium perfluorooctanoate which is an anionic fluorinated surfactant. Previous work (Cavallaro *et al.*, 2014b) proved that the lumen of HNTs modified with fluorinated surfactants showed a good affinity towards oxygen. The resistance to thermal degradation of the treated paper as well as the consolidation efficiency were determined by thermogravimetry (TG), which is an established technique for the characterization of composites (Rotaru *et al.*, 2008; Blanco *et al.*, 2012), nanoclay thermal behaviour (Duce *et al.*, 2015a) and the diagnostics of art-work materials (Badea *et al.*, 2011; Duce *et al.*, 2012, 2015b). Paper grammage (= paper density) data were compared with the loading results obtained by TG.

The treated papers were imaged by scanning electron microscopy (SEM) to demonstrate the structure at the mesoscopic scale, while the wettability was investigated by means of water contact angle measurements. The effect of the consolidation on the paper combustion was studied using differential scanning calorimetry (DSC). The knowledge acquired represents the starting point for designing a consolidation green protocol useful for increasing the protection ability and physico-chemical performance of paper artworks.

MATERIALS AND METHODS

Materials

Halloysite ($Al_2Si_2O_5(OH)_4 \cdot 2H_2O$, HNT) with a specific surface area of 65 $m^2\ g^{-1}$ and a specific gravity of 2.53 g cm^{-3} was from Sigma (Dragon Mine, Utah, USA). Perfluorooctanoic acid (PFC8H), from Fluka was crystallized from carbon tetrachloride and dried at room temperature. Its sodium salts (NaPFC8) were prepared by neutralization with an aqueous sodium hydroxide solution. The product was crystallized twice from an ice-cold solution and dried in a vacuum oven at 60°C for 4 days before use. The paper sample was cellulose-based from Albet® (thickness-0.16 mm and a water capillary raise of >178 mm h^{-1}).

Preparation of f-HNTs

The modification of the lumen of HNTs with NaPFC8 was carried out as reported elsewhere (Cavallaro *et al.*, 2014b). Briefly, an aqueous surfactant solution (0.1 mol kg^{-1}) containing 0.02 g cm^{-3} of HNTs was prepared. After magnetic stirring for ~1 day, the solid was separated by centrifugation and rinsed several times with water until the surface tension of the supernatant was close to the value of water (~72 mN m^{-1}). This procedure ensures that all the excess free surfactant is removed. The solid obtained (f-HNTs) was dried at 80°C for 1 week. The NaPFC8 loading of 0.91% was determined by means of thermogravimetry (TG).

Paper treatment

The HNT and f-HNT aqueous dispersions (1.0 wt.%) were prepared, sonicated for 1 h and kept under magnetic stirring overnight. The paper samples were cut into rectangular shapes (40 mm × 8 mm) and immersed in the aqueous mixture prepared for 24 h at 20°C. The treated samples were dried at 35°C under vacuum. Note that the HNT loading onto the paper can be controlled by the concentration of aqueous dispersions (Cavallaro *et al.*, 2014a). A blank experiment was carried out by treating a paper sample with water using the same protocol as above, for the sake of simplicity; this sample is referred to as "paper" in the results and discussion section. Modification of the HNT lumen as well as the paper impregnation is presented schematically in Fig. 1.

https://doi.org/10.1180/claymin.2016.051.3.01 Published online by Cambridge University Press

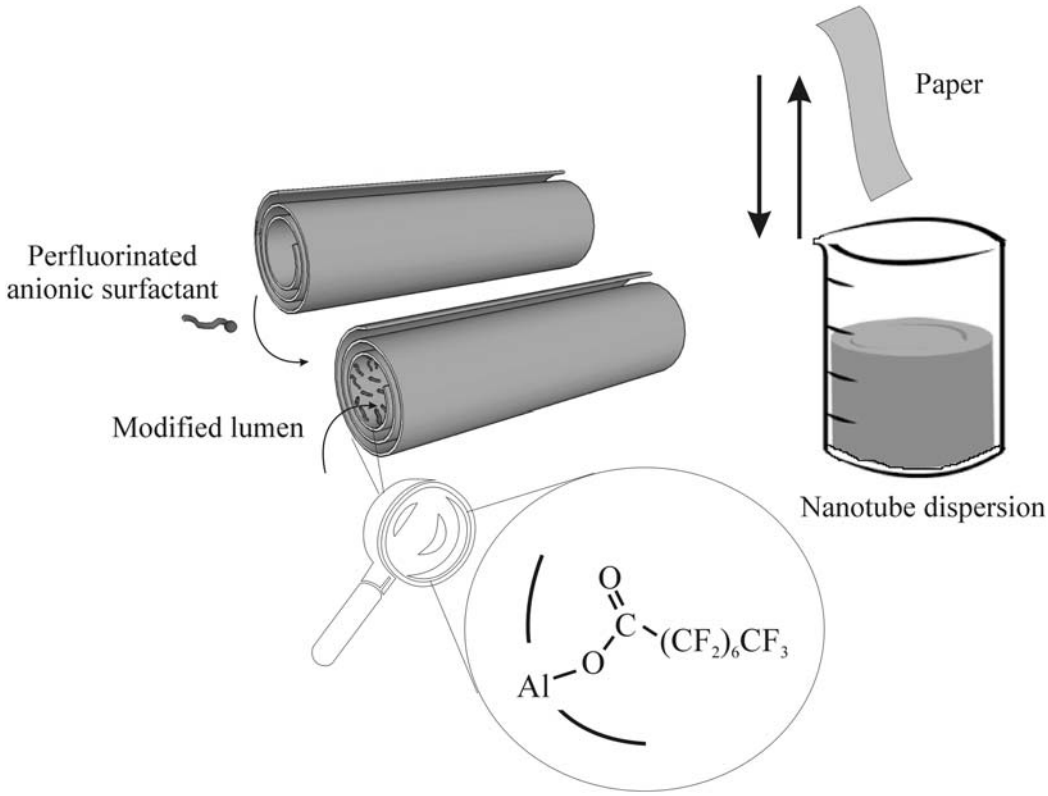

FIG. 1. Schematic representation of both modification of the HNT lumen and paper treatment.

Scanning electron microscopy

The morphology of nanocomposites was studied using an ESEM FEI QUANTA 200F microscope coupled with an energy dispersive X-ray spectrometer (EDAX) used to determine the elemental analysis. The sample surface was coated with gold in argon by means of an Edwards Sputter Coater S150A to avoid charging under the electron beam. The measurements were carried out in high vacuum mode ($<6 \times 10^{-4}$ Pa) for simultaneous secondary electrons; the energy of the beam was 25 kV and the working distance was 10 mm. The beam exposure time for EDAX was 200 s.

Paper grammage determination

The paper samples, cut in a rectangular shape (~40 mm × 8 mm), were vacuum dried and weighed (±0.01 mg). The area was determined by measuring the size with a caliper (±0.05 mm). Grammage (Gr) was calculated for treated and untreated paper as the ratio between the weight and the area.

Thermogravimetry

The TG experiments were performed using a Q5000 IR apparatus (TA Instruments) under a nitrogen flow of 25 cm^3 min^{-1} for the sample and 10 cm^3 min^{-1} for the balance. The weight of each sample was ~5 mg. The sample was heated from room temperature to 600°C at a rate of 10°C min^{-1}. The temperature calibration was carried out by means of Curie temperatures of standards (nickel, cobalt and their alloys). The experiments were repeated three times on each sample.

Differential scanning calorimetry

The enthalpy (ΔH) of combustion under static air conditions for paper before and after each treatment was determined by using the TA Instruments DSC (2920 CE) in the range from 150 to 550°C at a heating rate of 10°C min^{-1}. The sample mass was ~5 mg. The calibration was carried out using an indium standard. The reproducibility of the ΔH results was estimated by repeating the experiment three times.

https://doi.org/10.1180/claymin.2016.051.3.01 Published online by Cambridge University Press

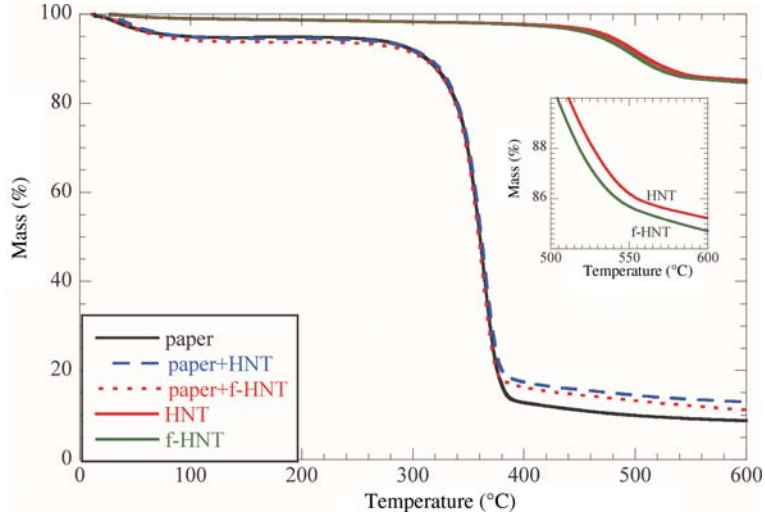

FIG. 2. TG curves under nitrogen for pristine and treated paper samples. The inset reports TG curves for HNTs and f-HNTs in a high-temperature range.

Wettability

Contact-angle studies were performed by means of an optical contact angle apparatus (OCA 20, Data Physics Instruments). The contact angle (θ) of water in air was measured by means of the sessile drop method by placing a droplet of 6.0 ± 0.5 μL onto the surface. The temperature was set at 25.0°C ± 0.1°C for the support and the injecting syringe. Images were collected at a rate of 25 frames s^{-1}. The initial contact angle value (θ_i) was extrapolated from the θ *vs.* time (*t*) trend using the procedure reported in the literature (Cavallaro *et al.*, 2013b). Five measurements were carried out on each sample.

Dynamic mechanical analysis

Tensile tests were performed by means of a DMA Q800 instrument (TA Instruments) under a stress ramp

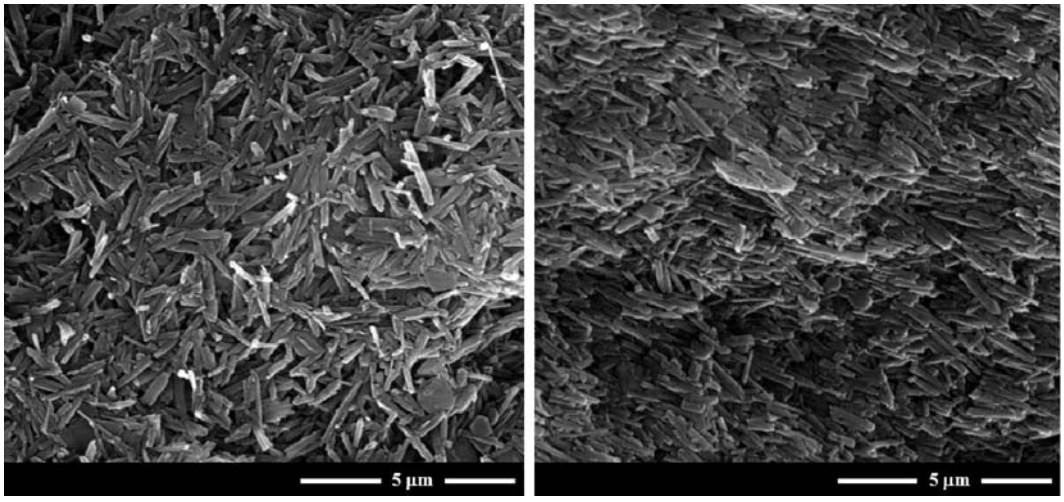

FIG. 3. SEM images for HNTs (left) and f-HNTs (right).

https://doi.org/10.1180/claymin.2016.051.3.01 Published online by Cambridge University Press

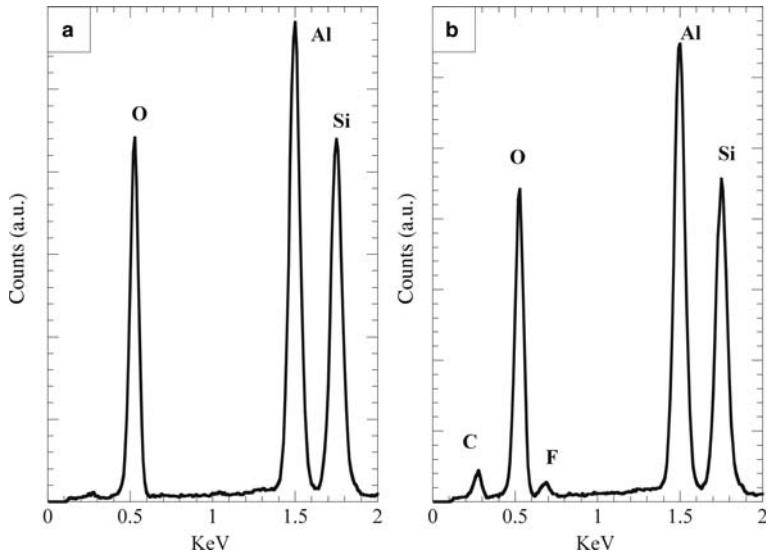

FIG. 4. EDAX spectra of HNTs (a) and f-HNTs (b).

of 1 MPa min^{-1} at 26.0°C ± 0.5°C. Tensile strength (defined as the tensile stress at which the material fractures (σr)) and the percent elongation at break (ε%) were determined. The reproducibility was checked by repeating the experiment five times.

RESULTS AND DISCUSSION

Characterization of f-HNTs

The amount of fluorinated surfactant loaded onto the HNT lumen was estimated from thermogravimetric analysis (Fig. 2). The surfactant degradation step is not clearly identified in the hybrid material because of the low degree of functionalization of HNT surfaces, while the mass loss occurring at ~500°C is attributed to the expulsion of two water molecules from the halloysite interlayer. On the other hand, the residual mass at 600°C for f-HNTs was less than that for HNTs indicating the presence of surfactant in the lumen of halloysite. In particular, a surfactant loading of ~0.91% (see inset in Fig. 2) was estimated. This value is far less than the maximum loading ability of HNTs based on geometric consideration (~10% of the nanoclay volume) but it agrees with the predicted result of 0.9% for a monolayer at the alumina–water interface, and with our previous findings (0.86%) (Cavallaro *et al.*, 2014b). From TG experiments it turned out that the water loss up to 150°C, ~1%, was not influenced by the HNT modification.

The morphology of pristine and fluorinated HNTs was investigated by means of SEM (Fig. 3). The tubular morphology is clearly seen for both HNTs and f-HNTs and therefore it is preserved after the adsorption of perfluorinated surfactants. The outer radius and the length of f-HNTs are comparable to those observed for the pristine HNTs samples. This confirms that the preparation method did not cause a separation or a selection of nanotubes based on their size. The EDAX spectra were also recorded for HNTs and f-HNTs. As shown in Fig. 4, the f-HNTs sample is characterized by the fluorine and carbon peaks that reflect the presence of fluorinated alkyl chains.

Paper treatment with HNTs and f-HNTs: efficiency and morphology

The addition of tubular nanoparticles to improve the performance of a polymeric matrix is a well established strategy and several aspects can influence the properties of the material obtained (Du *et al.*, 2006; Cavallaro *et al.*, 2011a, 2013a). To evaluate the loading of nanoclay into the paper samples (L%) two different procedures were employed: (1) grammage (Gr) determination and (2) TG investigations. The specific mass of paper before and after each treatment is provided in Table 1. The increase in the Gr values is an indication of the success of the treatments. The L% can be calculated as $100(Gr_T - Gr_P)/Gr_P$ where the

https://doi.org/10.1180/claymin.2016.051.3.01 Published online by Cambridge University Press

Table 1. Grammage and halloysite loading data.

	Gr (g m^{-2})	L%
Paper	62.2	
Paper + HNTs	67.6	8.7[a] ; 5.9[b]
Paper + f-HNTs	65.2	4.8[a] ; 3.5[b]

[a]From Gr data
[b]From TGA data

subscripts T and P refer to treated and pristine paper samples, respectively. The results (Table 1) indicate that the HNT loading is larger than that for f-HNTs. The TG curves under nitrogen show that the thermal degradation path of the paper sample is scarcely influenced by the HNT or f-HNT presence as the onset of the single degradation step (occurring in the temperature range between 300 and 400°C) is independent of the treatment (Fig. 2). Similar results are reported for paper treatment with HNTs and modified cellulose (Cavallaro *et al.*, 2014a). The residual mass at 600°C is proof of the incorporation of nanoclay into the cellulose matrix and this has allowed us to calculate the L% (Table 1) by using the rule of mixtures. The L% values from TG are in good agreement with those from Gr data. Note also that the paper treatment does not alter the water content, being ~5% in all samples.

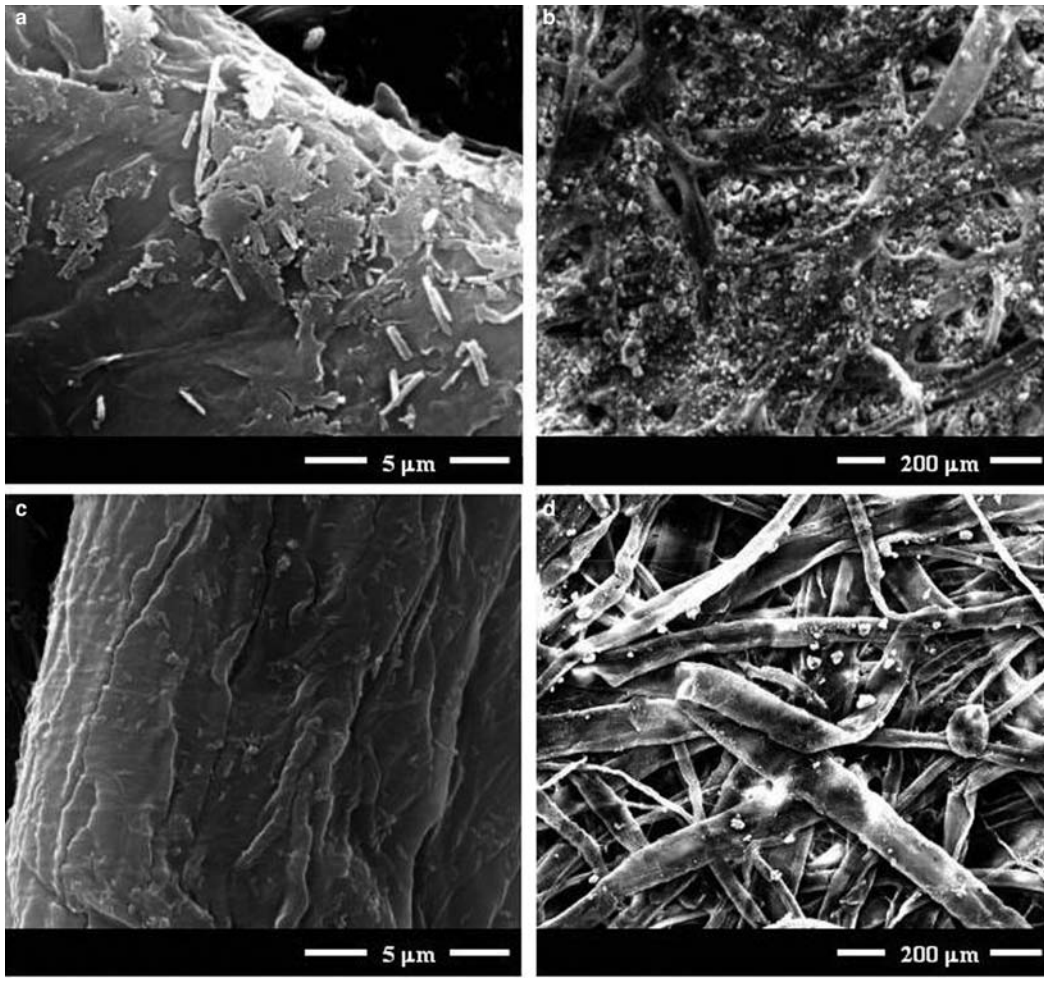

Fig. 5. SEM images for paper consolidated with aqueous suspensions of HNTs (a,b) and f-HNTs (c,d).

https://doi.org/10.1180/claymin.2016.051.3.01 Published online by Cambridge University Press

Besides the loading of nanoparticles, another key parameter to ensure the improvement of physico-chemical properties is the filler distribution. Although the amounts of HNT and f-HNT entrapped in the paper are comparable, a different nanoparticles distribution is observed by SEM in the treated paper samples (Fig. 5). The pristine HNTs form mainly clusters that are entrapped within the fibrous cellulose structure. By contrast, f-HNTs appear more compatible with the cellulose matrix showing a uniform distribution in the paper structure. Furthermore, the images with the largest magnification show that HNTs are deposited on the surface of the paper fibres while f-HNTs are embedded in the cellulose matrix. Such a different morphology might be related to the different charge of the nanoparticle, which is greater for the f-HNTs due to the partial neutralization of positive alumina sheet charge by the anionic surfactant (Cavallaro *et al.*, 2014b).

Effect of HNTs and f-HNTs on paper properties

For long-term conservation of paper-based artwork as well as for packaging applications, the water droplets interaction at the paper–air interface assumes a strategic role. The wettability and water-droplet adsorption kinetics were investigated by time-resolved contact-angle measurements. The water contact-angle values (θ) as a function of time until the droplets are fully absorbed by the paper are given in Fig. 6. The paper + HNT shows no strong alteration of interactions with the water droplet compared to untreated paper, whilst the addition of f-HNTs not only increases the θ values but it also slows down the water absorption. A quantitative analysis of the θ *vs. t* curves can be done by means of the following equation (Farris *et al.*, 2011)

$$\theta = \theta_i \exp(k\, t^n) \qquad (1)$$

where θ_i is the contact angle at $t = 0$, k is a measure of the process rate and n assumes fractional values ascribable to the absorption ($n = 0$) and/or spreading ($n = 1$) mechanism.

The best fits of the experimental θ *vs. t* curves (Fig. 6) provided the fitting parameters in Table 2. The θ_i changes indicate that the surface hydrophilicity follows the order paper > paper + HNT > paper + f-HNT. The alteration in wettability can reflect two aspects: (1) changing the chemical nature of the surface (Aulin *et al.*, 2008; Jin *et al.*, 2011); and/or (2) variation of the surface roughness (Marmur, 2008; Liu *et al.*, 2010). Because the θ_i of pristine HNTs is 20° (Zhao *et al.*, 2015), the θ_i increase observed in the paper + HNT sample should be ascribed to the surface-roughness improvement, which is in agreement with SEM data. For f-HNTs the hydrophobization and the roughness enhancement may induce synergistic effects in obtaining a less hydrophilic paper surface. It is interesting to note that both the rate-related constant (k) and the exponent *n* are not altered by addition of HNTs while f-HNTs decrease, by a factor of 2, the k value and changes the *n* value. This result indicates that f-HNTs,

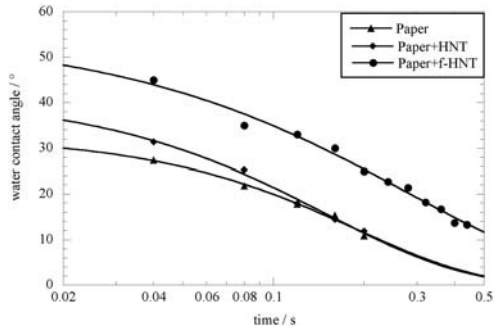

FIG. 6. Water-contact angle dependence on time for pristine and treated paper samples. Lines are best fits according to equation 1.

TABLE 2. Water-contact angle results.

	θ_i (°)	k	*n*
Paper	33 ± 4	−6 ± 2	1.0 ± 0.3
Paper + HNT	42 ± 3	−6 ± 2	0.9 ± 0.3
Paper + f-HNT	55 ± 5	−2.6 ± 0.2	0.76 ± 0.12

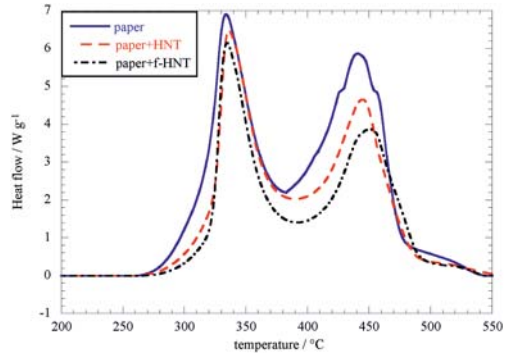

FIG. 7. DSC curves under static air for pristine and treated paper samples.

https://doi.org/10.1180/claymin.2016.051.3.01 Published online by Cambridge University Press

TABLE 3. Combustion data[a].

	ΔHc (kJ g^{-1})	T_{on} (°C)	T_1 (°C)	T_2 (°C)
Paper	6.02	295	331	438
Paper + HNT	5.12	297	333	442
Paper + f-HNT	4.88	318	332	444

[a]Errors are: 4% on enthalpy and 2% on temperature.

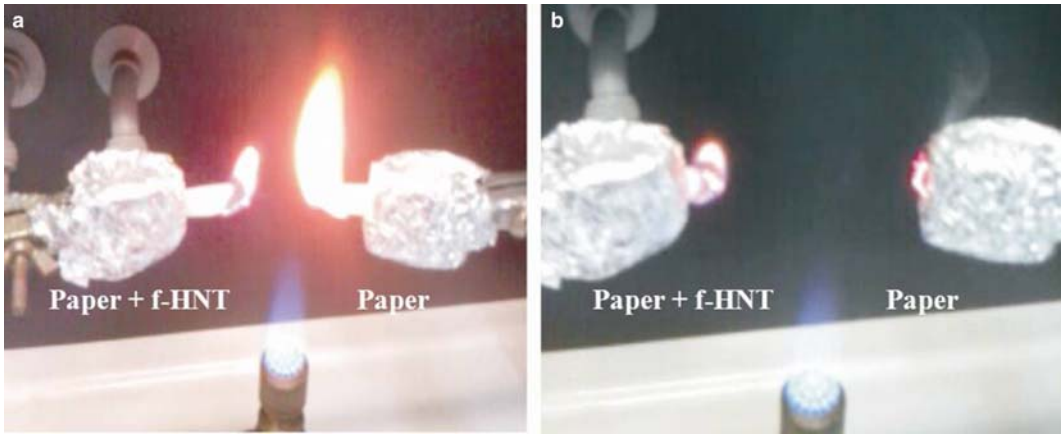

FIG. 8. Images of untreated paper and of paper treated with f-HNT after: (a) 4 and (b) 8 s from the start of paper burning.

even if it is less concentrated in the paper matrix, influences to a greater extent the paper interactions with a water droplet.

To elucidate the effect of the paper treatments on combustion in static air, DSC experiments were performed under these conditions and the results are shown in Fig. 7. Two degradation steps are highlighted clearly at ~330 and 440°C, respectively. Based on literature reports (Priegert *et al.*, 2015), the first step is related to cellulose degradation while the second is due to slow oxidative degradation of lignin. Table 3 reports onset temperature for the degradation process (T_{on}), combustion heat (ΔHc) and the temperatures at DSC peaks for each degradation step (T_1, T_2). The T_{on} values demonstrate an efficient stabilization effect of f-HNTs while HNTs alter just slightly the combustion process of paper to higher temperatures. The flame-retardant properties are well established by comparing the ΔHc value for paper before and after treatments. The significant decrease (>20%) indicates the thermal stabilization of paper in the presence of f-HNTs. Going further, the second step of the degradation is shifted to higher temperatures and proves that oxidation of lignin is retarded by HNTs and even more by f-HNTs. The better flame-retardant effect of modified nanotubes compared to pristine HNTs could be explained by taking into account the gas entrapment ability of f-HNTs (Cavallaro *et al.*, 2014b). Some snapshots of treated and untreated paper samples during burning show the flame-retardant ability of the

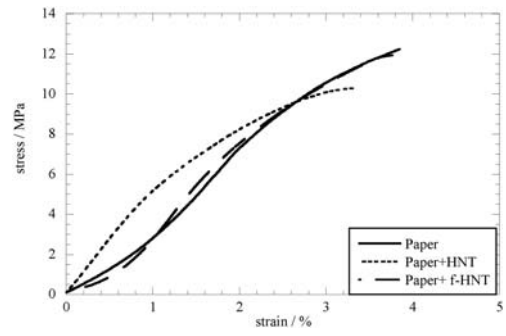

FIG. 9. Stress *vs.* strain curves for untreated and treated papers.

https://doi.org/10.1180/claymin.2016.051.3.01 Published online by Cambridge University Press

TABLE 4. Tensile properties of untreated and treated papers.

	σ_r (MPa)	ε%
Paper	11.8 ± 0.2	3.8 ± 0.1
Paper + HNT	10.2 ± 0.4	3.3 ± 0.3
Paper + f-HNT	12.2 ± 0.4	3.9 ± 0.2

treatment (Fig. 8). In particular, for a specimen (~40 mm × 8 mm × 0.16 mm) the burning rates are roughly 5 and 3 mm s^{-1} for untreated and treated paper, respectively.

Finally, the influence of HNTs and f-HNTs on the tensile properties of the paper was investigated by means of DMA experiments. Figure 9 shows the stress *vs*. strain curves for both untreated and treated papers. As observed in a previous study (Cavallaro *et al.*, 2014a), the addition of pristine HNTs does not affect significantly either the σ_r or ε% values (Table 4). Similar results were obtained for paper impregnated with f-HNTs (Table 4) indicating that the addition of modified HNTs does not improve the mechanical performance of the cellulose fibres.

CONCLUSIONS

Halloysite nanotubes with a fluorinated lumen were prepared successfully by exploiting the ionic exchange with a perfluorinated surfactant. The effect of addition of HNTs and f-HNTs to cellulose-based paper was investigated. A uniform distribution of nanoparticles into the paper sample was achieved in all cases and the visual aspect of the paper was not altered. The distribution and morphology of nanotubes within the fibres depend on the halloysite functionalization. Halloysite nanotubes with perfluorinated lumen are very promising materials because they confer interesting flame-retardant properties on the paper due to their gas-entrapment ability. Moreover, the wettability and water absorption behaviour can be tuned by HNT or f-HNT treatment.

ACKNOWLEDGEMENTS

The present study was supported financially by the University of Palermo, PRIN 2010-2011 (prot. 2010329WPF), FIRB 2012 (prot. RBFR12ETL5) and PON-TECLA (PON03PE_00214_1).

REFERENCES

Aulin C., Shchukarev A., Lindqvist J., Malmström E., Wågberg L. & Lindström T. (2008) Wetting kinetics of oil mixtures on fluorinated model cellulose surfaces. *Journal of Colloid and Interface Science*, **317**, 556–567.

Badea E., Della Gatta G. & Budrugeac P. (2011) Characterisation and evaluation of the environmental impact on historical parchments by differential scanning calorimetry. *Journal of Thermal Analysis and Calorimetry*, **104**, 495–506.

Blanco I., Abate L., Bottino F.A. & Bottino P. (2012) Thermal degradation of hepta cyclopentyl, mono phenyl-polyhedral oligomeric silsesquioxane (hcp-POSS)/polystyrene (PS) nanocomposites. *Polymer Degradation and Stability*, **97**, 849–855.

Cavallaro G., Lazzara G. & Milioto S. (2011a) Dispersions of nanoclays of different shapes into aqueous and solid biopolymeric matrices. Extended physicochemical study. *Langmuir*, **27**, 1158–1167.

Cavallaro G., Donato D.I., Lazzara G. & Milioto S. (2011b) Films of halloysite nanotubes sandwiched between two layers of biopolymer: from the morphology to the dielectric, thermal, transparency, and wettability properties. *The Journal of Physical Chemistry C*, **115**, 20491–20498.

Cavallaro G., Lisi R., Lazzara G. & Milioto S. (2013a) Polyethylene glycol/clay nanotubes composites. *Journal of Thermal Analysis and Calorimetry*, **112**, 383–389.

Cavallaro G., Lazzara G. & Milioto S. (2013b) Sustainable nanocomposites based on halloysite nanotubes and pectin/polyethylene glycol blend. *Polymer Degradation and Stability*, **98**, 2529–2536.

Cavallaro G., Lazzara G., Milioto S. & Parisi F. (2014a) Halloysite nanotubes as sustainable nanofiller for paper consolidation and protection. *Journal of Thermal Analysis and Calorimetry*, **117**, 1293–1298.

Cavallaro G., Lazzara G., Milioto S., Palmisano G. & Parisi F. (2014b) Halloysite nanotube with fluorinated lumen: Non-foaming nanocontainer for storage and controlled release of oxygen in aqueous media. *Journal of Colloid and Interface Science*, **417**, 66–71.

Cavallaro G., Lazzara G., Milioto S., Parisi F. & Sanzillo V. (2014c) Modified halloysite nanotubes: nanoarchitectures for enhancing the capture of oils from vapor and liquid phases. *ACS Applied Materials & Interfaces*, **6**, 606–612.

Cavallaro G., Lazzara G., Milioto S., Parisi F. & Sparacino V. (2015) Thermal and dynamic mechanical properties of beeswax-halloysite nanocomposites for consolidating waterlogged archaeological woods. *Polymer Degradation and Stability*, **120**, 220–225.

Du M., Guo B. & Jia D. (2006) Thermal stability and flame retardant effects of halloysite nanotubes on poly

https://doi.org/10.1180/claymin.2016.051.3.01 Published online by Cambridge University Press

(propylene). *European Polymer Journal*, **42**, 1362–1369.

Duce C., Ghezzi L., Onor M., Bonaduce I., Colombini M., Tine' M. & Bramanti E. (2012) Physico-chemical characterization of protein–pigment interactions in tempera paint reconstructions: casein/cinnabar and albumin/cinnabar. *Analytical and Bioanalytical Chemistry*, **402**, 2183–2193.

Duce C., Vecchio Ciprioti S., Ghezzi L., Ierardi V. & Tinè M. (2015a) Thermal behavior study of pristine and modified halloysite nanotubes. *Journal of Thermal Analysis and Calorimetry*, **121**, 1011–1019.

Duce C., Orsini S., Spepi A., Colombini M.P., Tiné M.R. & Ribechini E. (2015b) Thermal degradation chemistry of archaeological pine pitch containing beeswax as an additive. *Journal of Analytical and Applied Pyrolysis*, **111**, 254–264.

Fakhrullina G.I., Akhatova F.S., Lvov Y.M. & Fakhrullin R.F. (2015) Toxicity of halloysite clay nanotubes in vivo: a *Caenorhabditis elegans* study. *Environmental Science: Nano*, **2**, 54–59.

Farris S., Introzzi L., Biagioni P., Holz T., Schiraldi A. & Piergiovanni L. (2011) Wetting of biopolymer coatings: contact angle kinetics and image analysis investigation. *Langmuir*, **27**, 7563–7574.

Fix D., Andreeva D.V., Lvov Y.M., Shchukin D.G. & Möhwald H. (2009) Application of inhibitor-loaded halloysite nanotubes in active anti-corrosive coatings. *Advanced Functional Materials*, **19**, 1720–1727.

Gorrasi G., Pantani R., Murariu M. & Dubois P. (2014) PLA/Halloysite nanocomposite films: water vapor barrier properties and specific key characteristics. *Macromolecular Materials and Engineering*, **299**, 104–115.

Hanid N.A., Wahit M.U., Guo Q., Mahmoodian S. & Soheilmoghaddam M. (2014) Development of regenerated cellulose/halloysites nanocomposites via ionic liquids. *Carbohydrate Polymers*, **99**, 91–97.

Havlínová B., Katuščák S., Petrovičová M., Maková A. & Brezová V. (2009) A study of mechanical properties of papers exposed to various methods of accelerated ageing. Part I. The effect of heat and humidity on original wood-pulp papers. *Journal of Cultural Heritage*, **10**, 222–231.

Jana K. (2009) Mechanism of autoxidative degradation of cellulose. *Restaurator*, **18**, 163–176.

Jin C., Yan R. & Huang J. (2011) Cellulose substance with reversible photo-responsive wettability by surface modification. *Journal of Materials Chemistry*, **21**, 17519–17525.

Joshi A., Abdullayev E., Vasiliev A., Volkova O. & Lvov Y. (2013) Interfacial modification of clay nanotubes for the sustained release of corrosion inhibitors. *Langmuir*, **29**, 7439–7448.

Joussein E., Petit S., Churchman G.J., Theng B., Righi D. & Delvaux B. (2005) Halloysite clay minerals – a review. *Clay Minerals*, **40**, 383–426.

Liu M., Jia Z., Liu F., Jia D. & Guo B. (2010) Tailoring the wettability of polypropylene surfaces with halloysite nanotubes. *Journal of Colloid and Interface Science*, **350**, 186–193.

Liu M., Wu C., Jiao Y., Xiong S. & Zhou C. (2013) Chitosan-halloysite nanotubes nanocomposite scaffolds for tissue engineering. *Journal of Materials Chemistry B*, **1**, 2078–2089.

Luo Z., Song H., Feng X., Run M., Cui H., Wu L., Gao J. & Wang Z. (2013) Liquid crystalline phase behavior and sol–gel transition in aqueous halloysite nanotube dispersions. *Langmuir*, **29**, 12358–12366.

Lvov Y. & Abdullayev E. (2013) Functional polymer–clay nanotube composites with sustained release of chemical agents. *Progress in Polymer Science*, **38**, 1690–1719.

Lvov Y.M., Shchukin D.G., Mohwald H. & Price R.R. (2008) Halloysite clay nanotubes for controlled release of protective agents. *ACS Nano*, **2**, 814–820.

Makaremi M., De Silva R.T. & Pasbakhsh P. (2015) Electrospun nanofibrous membranes of polyacrylonitrile/halloysite with superior water filtration ability. *The Journal of Physical Chemistry C*, **119**, 7949–7958.

Marmur A. (2008) From hygrophilic to superhygrophobic: theoretical conditions for making high-contact-angle surfaces from low-contact-angle materials. *Langmuir*, **24**, 7573–7579.

Pasbakhsh P., Churchman G.J. & Keeling J.L. (2013) Characterisation of properties of various halloysites relevant to their use as nanotubes and microfibre fillers. *Applied Clay Science*, **74**, 47–57.

Priegert A.M., Siu P.W., Hu T.Q. & Gates D.P. (2015) Flammability properties of paper coated with poly (methylenephosphine), an organophosphorus polymer. *Fire and Materials*, **39**, 647–657.

Qiao J., Adams J. & Johannsmann D. (2012) Addition of halloysite nanotubes prevents cracking in drying latex films. *Langmuir*, **28**, 8674–8680.

Rotaru A., Nicolaescu I., Rotaru P. & Neaga C. (2008) Thermal characterization of humic acids and other components of raw coal. *Journal of Thermal Analysis and Calorimetry*, **92**, 297–300.

Shen J., Song Z., Qian X. & Ni Y. (2010) A review on use of fillers in cellulosic paper for functional applications. *Industrial and Engineering Chemistry Research*, **50**, 661–666.

Shutava T.G., Fakhrullin R.F. & Lvov Y.M. (2014) Spherical and tubule nanocarriers for sustained drug release. *Current Opinion in Pharmacology*, **18**, 141–148.

Soares N.F.F., Moreira F.K.V., Fialho T.L. & Melo N.R. (2012) Triclosan-based antibacterial paper reinforced with nano-montmorillonite: a model nanocomposite for the development of new active packaging. *Polymers for Advanced Technologies*, **23**, 901–908.

Soheilmoghaddam M., Wahit M.U., Mahmoudian S. & Hanid N.A. (2013) Regenerated cellulose/halloysite

https://doi.org/10.1180/claymin.2016.051.3.01 Published online by Cambridge University Press

nanotube nanocomposite films prepared with an ionic liquid. *Materials Chemistry and Physics*, **141**, 936–943.

Tankhiwale R. & Bajpai S.K. (2009) Graft copolymerization onto cellulose-based filter paper and its further development as silver nanoparticles loaded antibacterial food-packaging material. *Colloids and Surfaces B: Biointerfaces*, **69**, 164–168.

Vergaro V., Lvov Y.M. & Leporatti S. (2012) Halloysite clay nanotubes for resveratrol delivery to cancer cells. *Macromolecular Bioscience*, **12**, 1265–1271.

Wei W., Minullina R., Abdullayev E., Fakhrullin R., Mills D. & Lvov Y. (2014) Enhanced efficiency of antiseptics with sustained release from clay nanotubes. *RSC Advances*, **4**, 488–494.

Whitmore M.P. & Bogaard J. (2009) Determination of the cellulose scission route in the hydrolytic and oxidative degradation of paper. *Restaurator*, **15**, 26–45.

Zhao Y., Abdullayev E., Vasiliev A. & Lvov Y. (2013) Halloysite nanotubule clay for efficient water purification. *Journal of Colloid and Interface Science*, **406**, 121–129.

Zhao Y., Cavallaro G. & Lvov Y. (2015) Orientation of charged clay nanotubes in evaporating droplet meniscus. *Journal of Colloid and Interface Science*, **440**, 68–77.

https://doi.org/10.1180/claymin.2016.051.3.01 Published online by Cambridge University Press